Enhancements to the Work Ability of a High-Speed Motor Used in Machine Tools

Wawan Purwanto [1], Yusuf Dewantoro Herlambang [2], Kristine Mae Paboreal Dunque [3], Firoj Mulani [4], Dwi Sudarno Putra [1], Martias Martias [1]

[1]Department of Automotive Engineering, Engineering Faculty, Universitas Negeri Padang, Padang Indonesia
[2]Department of Mechanical Engineering, Politeknik Negeri Semarang, Semarang, Indonesia
[3]Department of Electrical engineering, University of Science and Technology of Southern Philippines Cagayan de Oro City, Philippines
[4]Departement of Electrical Engineering, Southern Taiwan University of Science and Technology, No.1, Nantai St., Tainan City 710301, Taiwan

Abstract – **This paper presents a strategy for maximizing the effectiveness of high-speed spindle motors in manufacturing equipment. Using the ideal design of the stator winding geometry, as calculated by the Taguchi method, we were able to increase the maximum torque and efficiency. The rotor slot geometry was optimized using a response surface to raise the starting torque and reduce the starting current. The objectives of this investigation were to come up with a strategy for designing high-speed spindle motors so that they have better performance in terms of starting torque, maximum torque, efficiency, and starting current. Spindle motor temperature rise was the focus of the thermal measurements. Finally, a working spindle motor prototype was built and tested to verify the results of the Finite element analysis (FEA). The validity of the suggested model is demonstrated by a comparison between experimental measurements and finite element findings. The total percentage of mistakes was close to 2%.**

Keywords – **Efficiency, machine tools, maximum torque, rotor, stator.**

1. Introduction

In recent years, the production of high-speed spindle motors has garnered considerable attention. This is due to the widespread use of motorized spindles in numerous industries [1]. High torque and efficiency are the primary challenges in fabricating spindle motors. In addition, beginning conditions, such as low starting current and high starting torque, are essential for fast response. Such as opinion of [2],[3],[4] to determine the electromagnetic force (EMF), it is necessary to do research on the stator winding geometry, including the stator length, stator slot geometry, the number of windings turns per slots, and the wire diameter. In addition, the EMF transfer from the stator winding to the rotor was influential in producing a high maximum torque and enhancing the spindle motor's efficiency.

Optimizing the winding structure of the stator geometry by analyzing the winding connections, pole numbers, and wire diameter with a finite element software may enhance the spindle motor's maximum torque and efficiency [5]. Previous research has successfully performed optimal design on stator configurations with various methods such as using response surface methodology (RSM) [5], multi-objective optimization [2], [6] and Ansys software [7], [8] to optimize the stator teeth width, yoke width, air-gap length, bore diameter, bridge distance, and slot openings. The subsequent stator winding design, which involves coil turns, winding configuration, and winding connection form for the high-efficiency motor was conducted by Rossi et al, [9]. Recently a study comparative technical and analysis of high efficiency in the commercial motor is presented by Ghosh et al, [10]. The rotor slot shape is a function to obtain quick starting of the spindle motor due to the impact of skin [11] and leakage flux concentration. Spindle motor the beginning conditions are improved as a direct consequence of the reduced rotor leakage reactance and EMF variations [12], [13].

Improving the starting torque through rotor slot design was conducted by Xu et al, [14]. After identifying the initial operation challenges, a high-power motor can be designed and evaluated using one of three possible solutions: deep bars, magnetic triangles, or a double cage [15]. Of these three options, the deep bars and twice cage objects raise starting torque while simultaneously decreasing starting current [12].

While there are various other cage rotor slot configurations in use, high-speed spindle motors typically employ the closed rotor slot design. One advantage involves a lessening of mechanical issues brought on by extremely fast motors [4], [6]. In addition, it utilizes efficient use of the skin's impact to achieve targets related to performance, for instance increased starting torque and decreased starting electrical current. The present investigation builds on previous studies by measuring and contrasting the efficiency of different designs for high-speed spindle motors to optimize their ability to operate. The purposes required a spindle motor with operating characteristics, such as high starting torque and low starting current for fast response, workload stability, and cost-effectiveness. The stator winding and rotor design were optimized using the Taguchi method and RSM in conjunction with FEA to reach the effectiveness targets of the motor. Besides electromechanical design considerations, thermal design is also crucial [16], especially for high-speed operation. The temperature rise of the spindle motor has typically been predicted using the thermal difference model, equivalent resistance thermal model, thermal difference and FEA, and power loss distribution model [13]. In the present study, the temperature rise of the spindle motor was obtained from temperature measurement of the spindle motor prototype. Finally, the proposed model of the spindle motor prototype was then manufactured and evaluated to confirm the accuracy of the findings from the simulation.

2. Material of the Motor

The fundamental parameters of the motor are summarized in Table 1, it has a rated power of 14 kW, four poles, a connection, which is 380 V, and 21000 rpm. We use electromagnetic silicon steel 35H250 for our stator. Figures 1 and 2 depict the component's B-H curves and stator core loss, respectively. The A region has the lowest concentration and maximum flux density in this type of material. However, in the B area (the high-saturated region), it has the lowest saturation flux density. Since current and core loss can be minimized in this region, it is where the material shines brightest.

Table 2 details the results of a finite element model (FEM) simulation of the spindle [12]. Based on the data presented in the table, the low performance and substantial losses experienced by the spindle motor are the result of excessive stator resistance. Further, the coil length must be reduced, the stator current density must be kept from increasing, the stator thermal load must be kept to a minimum, and the flux density must be distributed fairly across the coil area to maximize torque and efficiency.

Table 1. The high-speed motor specifications

Parameter	Value [mm]
Inner diameter of the stator	70
Outer diameter of the stator	120
Length of the stator core	120
Outer diameter of the rotor	69.3
Inner diameter of the rotor	38
Number of stator/rotor slot	36/32

Table 2. Industrial design of spindle performance

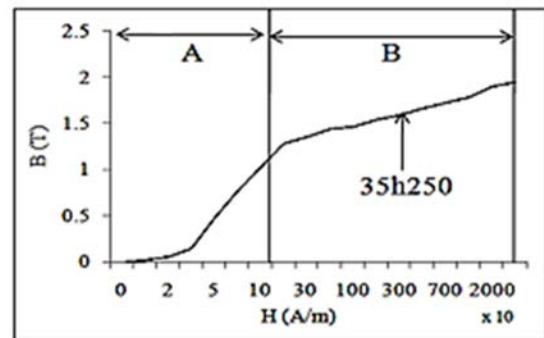| Parameter	Symbol	Values
Stator resistance [Ohm]	R_2	1.502
Stating current [A]	I_{st}	35.23
Stator current [A]	I_s	18.79
Stator current density [A/mm^2]	j_b	37.73
Stator thermal load [A^2/mm^3]	A_{so}	736.21
Copper loss stator winding [W]	P_{co}	1342.89
Total loss [W]	Σ_{loss}	2194.11
Starting torque [Nm]	T_{start}	0.95
Maximum torque [Nm]	T_{max}	2.38
Efficiency [%]	η	86.45

Figure 1. B-H curves source
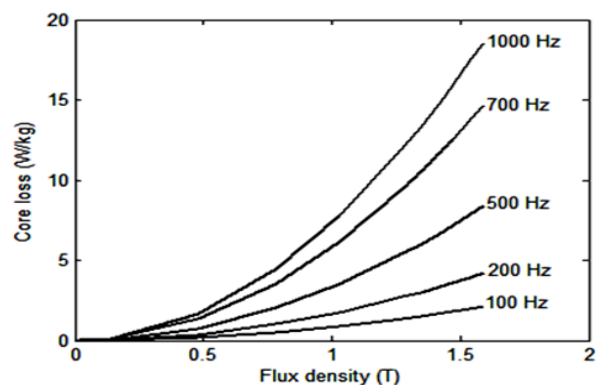
Figure 2. Core loss of core material 35h250

Table 3. Design levels classifications

Factors	Definition	-2	-1	0	1	2
A	Useful slot area (hs) [mm]	5.5	6.5	7.5	8.5	9.5
B	Slot higher width (bs_2) [mm]	4	4.4	4.8	5.2	5.6
C	Stator length (L) [mm]	110	120	130	140	150
D	Wire diameter (Wd) [mm]	0.381	0.511	0.643	0.767	0.912
E	Number of windings turns per slot (coil)	24	36	48	60	72

Table 4. Motor performance

Exp	hs [mm]	bs_2 [mm]	L [mm]	Wd [mm]	Coil	T_{max} (Nm)	Eff (%)
1	5.5	4	110	0.381	24	26.63	72.95
2	5.5	4.4	120	0.511	36	35.31	82.92
3	5.5	4.8	130	0.641	48	18.18	91.43
4	5.5	5.2	140	0.771	60	8.75	91.23
5	5.5	5.6	150	0.901	72	5.02	83.43
6	6.5	4	120	0.641	60	10.03	90.63
7	6.5	4.4	130	0.771	72	5.84	81.39
8	6.5	4.8	140	0.901	24	95.04	72.55
9	6.5	5.2	150	0.381	36	19.65	85.03
10	6.5	5.6	110	0.511	48	20.47	88.94
11	7.5	4	130	0.901	36	43.91	90.78
12	7.5	4.4	140	0.381	48	10.94	84.28
13	7.5	4.8	150	0.511	60	7.00	82.92
14	7.5	5.2	110	0.641	72	7.08	86.62
15	7.5	5.6	120	0.771	24	87.85	43.51
16	8.5	4	140	0.511	72	4.79	71.46
17	8.5	4.4	150	0.641	24	70.65	70.69
18	8.5	4.8	110	0.771	36	47.22	85.62
19	8.5	5.2	120	0.901	48	22.23	92.67
20	8.5	5.6	130	0.381	60	7.25	78.24
21	9.5	4	150	0.771	48	13.30	91.97
22	9.5	4.4	110	0.901	60	11.75	92.70
23	9.5	4.8	120	0.381	72	5.20	61.03
24	9.5	5.2	130	0.511	24	58.76	45.25
25	9.5	5.6	140	0.641	36	34.36	89.08

Table 5. ANOVA results of maximum torque

Factor	Definition	SS	d.f	Mean Sq	F	Prob > F	Contribution (%)
A	hs	569.89	4	142.47	1.24	0.42	3.42
B	bs_2	695.82	4	173.95	1.51	0.35	4.18
C	L	373.17	4	93.29	0.81	0.58	2.24
D	Wd	1399.40	4	349.85	3.04	0.15	8.41
E	$Coil$	13148.59	4	3287.15	28.57	0.0034	78.99
Error		460.14	4	115.04			
Total		16647.01	24				

Table 6. ANOVA results of efficiency

Factor	Definition	SS	d.f	Mean Sq	F	Prob > F	Contribution (%)
A	hs	271.38	4	67.85	1.54	0.34	6.13
B	bs_2	154.70	4	38.68	0.88	0.55	3.49
C	L	400.14	4	100.03	2.28	0.22	9.04
D	Wd	605.46	4	151.36	3.44	0.13	13.67
E	Coil	2821.09	4	705.27	16.04	0.01	63.70
error		175.85	4	43.96			
Total		4428.63	24				

Spindle motors with high beginning currents can have an impact on electrical load during start-up, which can in turn impair spindle safety and the reliability of the power grid. Therefore, the starting current and starting torque of the spindle motor can be improved by fine-tuning the rotor slot shape. Since the rotor's overall resistance has risen, the starting current has decreased, and the starting torque increased.

3. An Approach to Enhancing the Spindle Motor's Functionality

The purpose of obtaining a spindle motor exhibiting low stator resistance, stator thermal load, and stator winding core loss, in this research. Hence, the first step was to refine the stator winding geometry to reduce these conditions and improve the maximum torque and efficiency by using the Taguchi method. Then, RSM was adopted to refine the rotor slot geometry, thereby increasing starting torque and reducing starting current.

3.1. Refinement of Stator Winding Geometry

As can be seen in Figure 3, the Taguchi technique was implemented based on five components representing five design variables (labelled A, B, C, D, and E). There are five levels associated with every element. Table 3 lists the possible variations of factor levels. The performance of the spindle motor in the L_{25} (55) matrix experiment was predicted through FEA, the results are listed in Figure 4(a) for maximum torque and 4(b) for efficiency. Analysis of variance (ANOVA) was applied to investigate the relationship among the stator parameters, maximum torque, and efficiency. In the analysis, five factors and five levels of hs, bs_2, stator length, wire diameter, and the number of windings turned per slot were chosen. The results are listed in Tables 5 and 6. It showed a direct correlation between the wire diameter and the highest torque and efficiency. As can be shown in Tables 5 and 6, their use significantly improves both peak torque and efficiency. Figure 4 also displays the impact of these variables on peak torque and efficiency. Combinations of the (A3, B3, C1, D5, and E3) factor and level parameters allow for the highest possible efficiency and torque to be achieved.
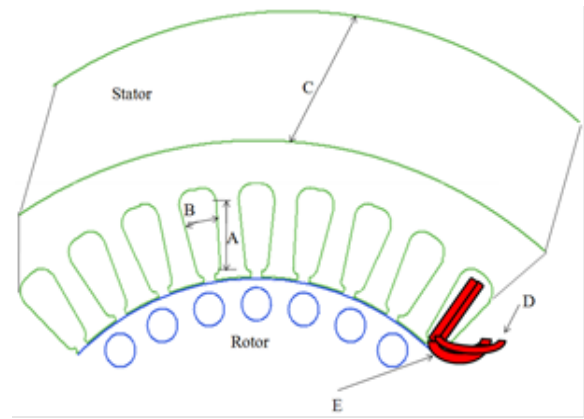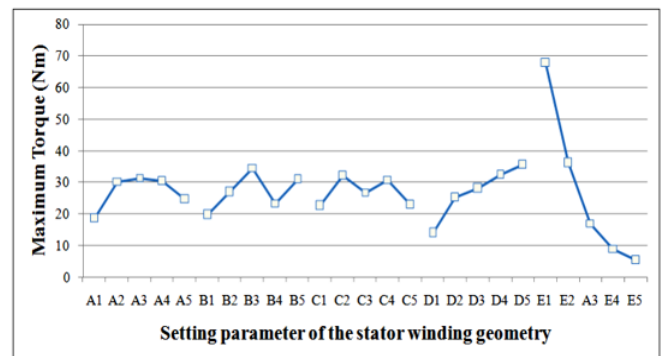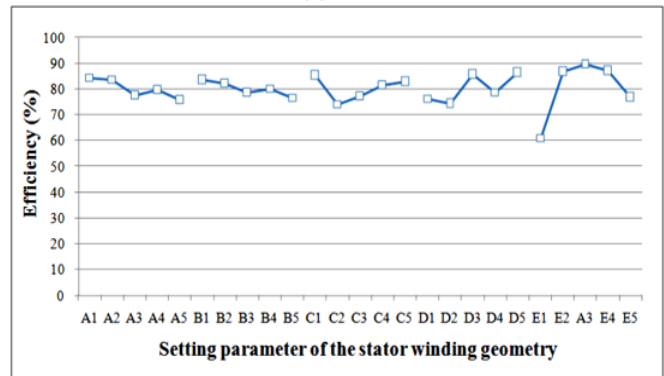

Figure 3. Definitions of factors

(a)

(b)

Figure 4. Main effect of an (a) maximum torque, and (b) efficiency

Table 7. Motor performance comparison

Symbol	Industrial	Taguchi
R_2 [Ohm]	1.502	0.414
I_{st} [A]	35.23	26.95
I_s [A]	18.79	15.22
j_b [A/mm^2]	37.73	11.77
A_{so} [A^2/mm^3]	736.21	265.59
P_{co} [W]	1342.89	241.46
Σ_{loss} [W]	2194.11	1025.52
T_{start} [Nm]	0.95	4.92
T_{max} [Nm]	2.38	7.45
η [%]	86.45	92.38

The proposed Taguchi technique spindle motor's performance was modelled using FEA software as used in study [5]. Table 7 summarizes the findings and comparison from industrial and proposed design. As we can see, the starting current, starting torque, stator current density, stator thermal load, copper loss in the stator winding, and overall loss all decreased as well, from 1,502 Ohm in the industrial design to 0.414 Ohm using the proposed approach. When compared to the practical designs of 0.95 Nm, the Taguchi approach improved this value to a whopping of 4.93 Nm. The maximum torque of 2.38 Nm increased to 7.45 Nm, and the efficiency of 86.46 % increased to 92.38 %. The results of the Taguchi method (versus industrial design) involve shorter stator length of 110 mm in Taguchi method rather than 120 mm in industrial design, lower the number of windings turns per slot of 48 in Taguchi method than 72 in industrial design with greater wire diameter 0.912 mm in Taguchi method instead of 0.511 mm in industrial design. The Taguchi method assists to increase the torque and efficiency of the spindle motor by decreasing the stator resistance, by reducing the coil length, and avoiding an increase in the stator current, stator current density, and stator thermal load.

3.2. Refinement of Stator Winding Geometry

In the present investigation, a squirrel cage rotor with a closed circular slot was utilized. The applications requiring a high-speed spindle motor benefit greatly from this design. It also successfully uses the skin effect to gain certain performance advantages including a strong starting torque, a higher maximum torque, better efficiency, and a lowered starting current, all of which are common mechanical issues in particularly high-speed motors. In addition, as can be shown in Figure 5(a)-(c), the RSM, design of experiments (DOE), and FEA were utilized to develop three types of closed rotor slots: round (Fig. 5a), round (Fig 5b), and oval (Fig 5c). Furthermore, these techniques enabled determining the right rotor slot type for the spindle motor. Figure 6 depicts the optimization procedure. As can be seen in Figure 7, the rotor geometry parameters are bs_1, bs_2, and hs determine the initial torque and starting current. Table 8 specifies the variables and goals of the experiment.

DOE indicates are generated from FEA simulation and used in the optimization process.

The FEA parameters and settings that optimized starting torque and reduced starting current are listed. When the number of findings from experiments fell short of the targets, the variable coordinate point was moved up to the optimal level of improvement. The central composite design method was implemented to probe the adjustment of a second-order model. After working out the coefficient by regression analysis, the optimal quadratic was found. An ideal blend was to be the result of this procedure. Once the study was completed, the ideal combination of parameters was used to conduct experiments and confirm the projected results. The projected result was confirmed when the result of the optimal design was barely inside the allowable limit. If this was not the case, we ran DOE repeatedly until we had the best possible design. inevitably can identify the ideal values for the variables in Table 9.
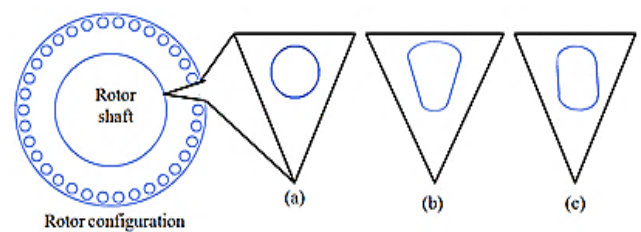

Figure 5. Closed rotor slots configuration, (a) circular closed, (b) round closed, (c) oval closed
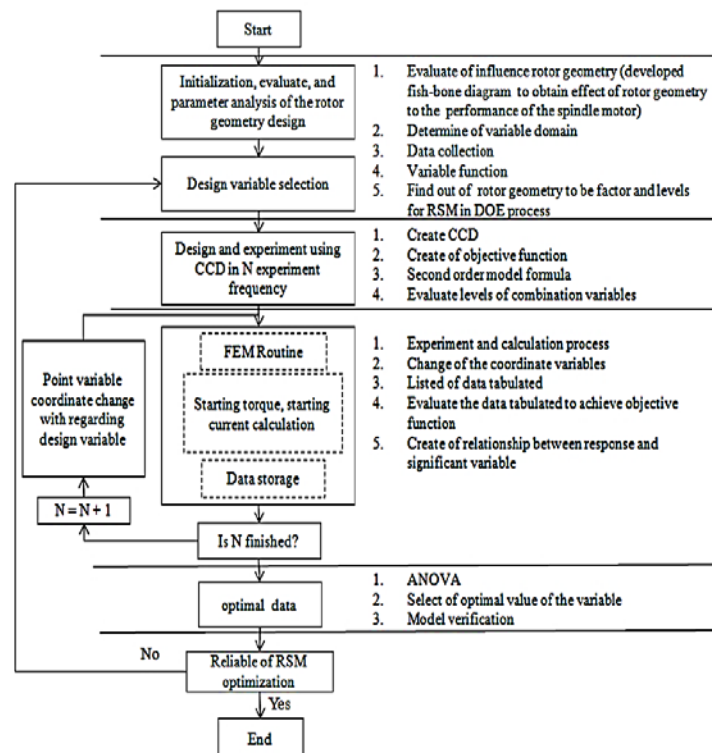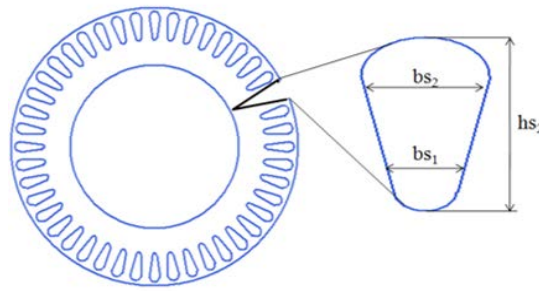

Figure 6. Optimization process

Figure 7. Rotor slot geometry parameters

Table 8. Experiment variable and objective functions

Rotor Slot	Parameters and levels	Maximum	Objective functions
		Minimum	
Circular closed [mm]	$0.1 \leq h_{s2} \leq 0.3$		Maximize $f_1(x) = T_{st}$
	$3 \leq b_{s1} \leq 5$		Minimize $f_2(x) = I_{st}$
	$3 \leq b_{s2} \leq 5$		
Round Closed [mm]	$2 \leq h_{s2} \leq 3$		Subject to:
	$1.5 \leq b_{s1} \leq 3$		$X_L \leq x \leq X_u$
	$3 \leq b_{s2} \leq 5$		x is variable vector, X_L and X_U is
Oval closed [mm]	$2 \leq h_{s2} \leq 3$		minimum and maximum limit of
	$2 \leq b_{s1} \leq 4$		the design variable
	$2 \leq b_{s2} \leq 4$		

Table 9. RSM results

Parameters	Circular closed	Round closed	Oval closed
hs_2 [mm]	0.2	2.48	2.89
bs_1 [mm]	4	1.69	4
bs_2 [mm]	4	5	4

Table 10. Performance comparison

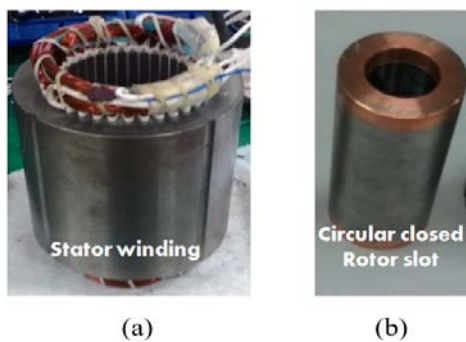| Symbol	Round closed	Oval closed	circular closed	Experiment	Error (%)
I_{st} [A]	24.24	25.35	23.13	23.03	0.43
T_{start} [Nm]	4.12	4.13	6.12	6.25	2.12
T_{max} [Nm]	7.82	7.82	7.86	7.86	0
η [%]	92.48	91.39	92.58	92.52	0.07

Figure 8. Prototype of the spindle motor, (a) stator, (b) rotor

4. Experimental Results and Discussions

A prototype of the suggested method's stator design is depicted in Figure 8(a) and rotor (Fig 8b), along with the circular, closed rotor slot. The impact of rotor slot design on spindle motor output is displayed in Table 10.

Starting current was lowest and starting torque was greatest for the circular closed rotor slot compared to the round and oval closed rotor slots [7]. Furthermore, the torque-speed comparisons of all designs are displayed in Figure 9. The experimental finding of 92.52% is an improvement in efficiency over the Taguchi method's industrial design result of 92.38%. Moreover, the maximum torque increased from 2.38 Nm in the industrial design to 7.45 Nm in the Taguchi method with an experimental result of 7.86 Nm. The starting torque increased from 0.95 Nm in the industrial design to 6.12 Nm in the RSM results for the circular closed rotor slot with an experimental result of 6.25 Nm. The starting current was reduced from 35.25 A in the industrial design to 23.13 A according to the RSM with a circular closed rotor slot, and an experimental result of 23.03 A. The preciseness of the suggested concept was confirmed by comparing the measured and simulated results of circular closed rotor slots.

As can be seen in Table 10, there is a good agreement between the measured findings and the simulated results, with an error of only about 2%. Figure 10 displays the prototype spindle motor's suggested model's stator current, output power, torque, and voltage.
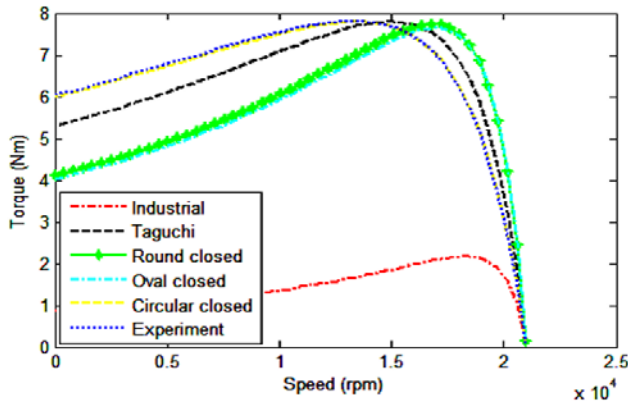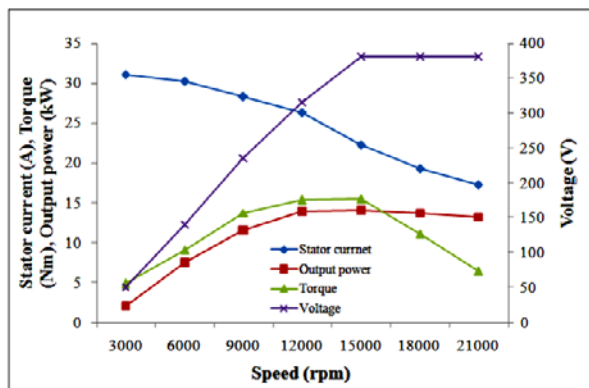

Figure 9. Torque-speed characteristics

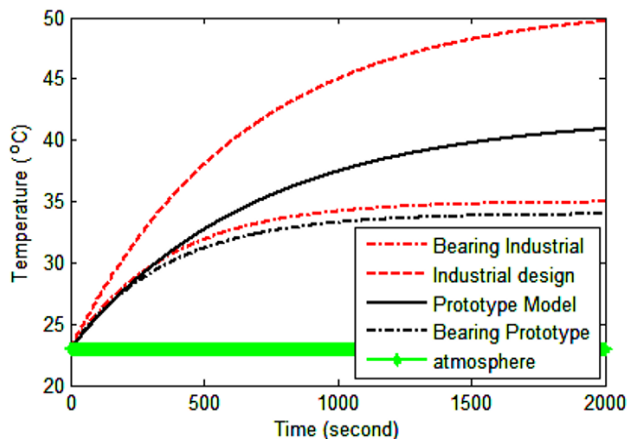*Figure 10. Performance characteristics of the prototype motor*

Figure 11. Temperature rises characteristics.

The thermal measurement shall be continued for the specific time, or until constant temperature rise has been reached [9], [16]. The temperature was measured in stator winding temperature and front bearing temperature.

The motor was coolant controlled at 23^0C with a flow rate 0.0288 m^3/s. The temperature rise characteristics for the prototype spindle motor are shown in Figure 11. The proposed model generated a lower temperature rise compared with the industrial design. The temperature rise was approximately 41 ^{0}C at the stator winding and 33 ^{0}C at the bearing in the proposed model, whereas the industrial design indicated a rise of 50 ^{0}C at the stator winding and 34^0C at the bearing.

5. Conclusion

In this research, we offer a strategy for increasing the efficiency of a high-speed spindle motor used in machine tools. To increase maximum torque and efficiency, the stator winding shape was initially refined using the Taguchi method. The RSM was also used to adjust the arrangement of the slots inside of the rotor. subsequently improve starting torque and decrease starting current, rotor slots with circular, round, and oval closures were implemented. To validate the computer modelling accomplishments, a physical replica of the stator geometry and a rotor with a circular closed slot were constructed and tested. The measured results of the circular closed rotor slot are generally consistent with the simulated results, with an approximate 2% range of error. The proposed model's thermal evaluation was under the critical point of temperature and lower than that of the industrial design. The proposed model shows a high starting torque, improved maximum torque and efficiency, and a lower starting current, which make it ideal for high-speed spindle motors employed in machine tool operations.

References:

[1]. Li, J., Wang, Q., Sun, X., Qu, J., Qiu, A., Kang, W., & Ma, S. (2022). Research on the Effect of Spindle Speed on the Softening and Hardening Characteristics of the Axial Operating Stiffness of Machine Tool Spindle. *Lubricants*, *10*(7), 132. Doi: 10.3390/LUBRICANTS10070132

[2]. Xu, F., He, T. R., Zhu, Z. Q., Bin, H., Wu, D., Gong, L. M., & Chen, J. T. (2022). Comparison of 2-pole Slotted High-speed Motors with Toroidal and Tooth-coil Windings. In *2022 IEEE 5th International Electrical and Energy Conference (CIEEC)*, 3410-3415.IEEE.Doi: 10.1109/CIEEC54735.2022.9845996

[3]. Gupta, A., MacHavaram, R., Kshatriya, T., & Ranjan, S. (2020). Multi-Objective Design Optimization of a Three Phase Squirrel Cage Induction Motor for Electric Propulsion System using Genetic Algorithm. In *Proc. 2020 IEEE First International Conference on Smart Technologies for Power, Energy and Control (STPEC)*. Doi: 10.1109/STPEC49749.2020.9297776.

[4]. Purwanto, W., Risfendra, & Putra, D. S. (2018). Effect of stator slot geometry on high speed spindle motor performance. In *2018 international conference on information and communications technology (ICOIACT)*, 561–565. Doi: 10.1109/ICOIACT.2018.8350693.

[5]. Purwanto, W., Sugiarto, T., Maksum, H., Martias, M., Nasir, M., & Baharudin, A. (2019). Optimal design of rotor slot geometry to reduce rotor leakage reactance and increase starting performance for high-speed spindle motors. *Advances in Electrical and Electronic Engineering (AEEE)*, *17*(2), 96-105. Doi: 10.15598/AEEE.V17I2.3170.

[6]. Chen, H., Zhao, J., Wang, H., Zhang, Q., Luo, X., Xu, H., & Xiong, Y. (2022). Multi-objective optimum design of five-phase squirrel cage induction motor by differential evolution algorithm. *Energy Reports*, *8*, 51-62. Doi: 10.1016/J.EGYR.2022.09.098.

[7]. Aishwarya, M., & Brisilla, R. M. (2022). Design of Energy-Efficient Induction motor using ANSYS software. *Results in Engineering*, *16*, 100616. Doi: 10.1016/J.RINENG.2022.100616.

[8]. Yang, Y. et al. (2016). Design and comparison of interior permanent magnet motor topologies for traction applications. *IEEE Transactions on Transportation Electrification*, *3*(1), 86-97. Doi: 10.1109/TTE.2016.2614972.

[9]. Rossi, N., Matteazzi, N., Petti, G. L., Fazzini, L., Nuzzo, S., Barater, D., & Franceschini, G. (2021). Design and thermal assessment of a high performance electric motor for racing applications. In *2021 IEEE Workshop on Electrical Machines Design, Control and Diagnosis (WEMDCD)*, 52-57. IEEE. Doi: 10.1109/WEMDCD51469.2021.9425681.

[10]. Ghosh, P. K., Sadhu, P. K., Basak, R., & Sanyal, A. (2020). Energy efficient design of three phase induction motor by water cycle algorithm. *Ain Shams Engineering Journal*, *11*(4), 1139-1147. Doi: 10.1016/J.ASEJ.2020.01.017.

[11]. Payza, O., Demir, Y., & Aydin, M. (2018). Investigation of losses for a concentrated winding high-speed permanent magnet-assisted synchronous reluctance motor for washing machine application. *IEEE Transactions on Magnetics*, *54*(11), 1-5. Doi: 10.1109/TMAG.2018.2848881.

[12]. Purwanto, W., Maksum, H., Sugiarto, T., Risfendra, R., & Baharudin, A. (2019). Optimal Design of Stator Slot Geometry for High-Speed Spindle Induction Motor Applications. In *2019 International Conference on Information and Communications Technology (ICOIACT)*, 811-816. IEEE. Doi: 10.1109/ICOIACT46704.2019.8938493.

[13]. Dong, B., Wang, K., Han, B., & Zheng, S. (2019). Thermal analysis and experimental validation of a 30 kW 60000 r/min high-speed permanent magnet motor with magnetic bearings. *IEEE Access*, *7*, 92184-92192. Doi: 10.1109/ACCESS.2019.2927464.

[14]. Xu, F. et al. (2021). Influence of slot number on electromagnetic performance of 2-pole high-speed permanent magnet motors with toroidal windings. In *2020 Fifteenth International Conference on Ecological Vehicles and Renewable Energies (EVER)*, Monte-Carlo, Monaco. Doi: 10.1109/EVER48776.2020.9242986.

[15]. Chakrabarty, S., & Kanagaraj, R. (2021). Design, Simulation, and Analysis of Switched Reluctance Motor for High-Speed Applications. In *2021 National Power Electronics Conference (NPEC)*, 1-6. IEEE. Doi: 10.1109/NPEC52100.2021.9672508.

[16]. Appadurai, M., Raj, E. F. I., & Venkadeshwaran, K. (2021). Finite element design and thermal analysis of an induction motor used for a hydraulic pumping system. *Materials Today: Proceedings*, *45*, 7100-7106. Doi: 10.1016/J.MATPR.2021.01.944.